ELSEVIER

Contents lists available at ScienceDirect

Materials & Design

journal homepage: www.elsevier.com/locate/matdes



Electromagnetic wave-absorbing behavior of soft-magnetic medium entropy alloys with BCC/L2₁ coherent microstructure



Zhiyao Ji^a, Qing Wang^{a,*}, Zhenhua Wang^a, Yuping Duan^{a,*}, Chuang Dong^a, Peter K. Liaw^b

^a Engineering Research Center of High Entropy Alloy Materials (Liaoning Province), Key Laboratory of Materials Modification by Laser, Ion and Electron Beams (Ministry of Education), School of Materials Science and Engineering, Dalian University of Technology, Dalian 116024, Liaoning, China

HIGHLIGHTS

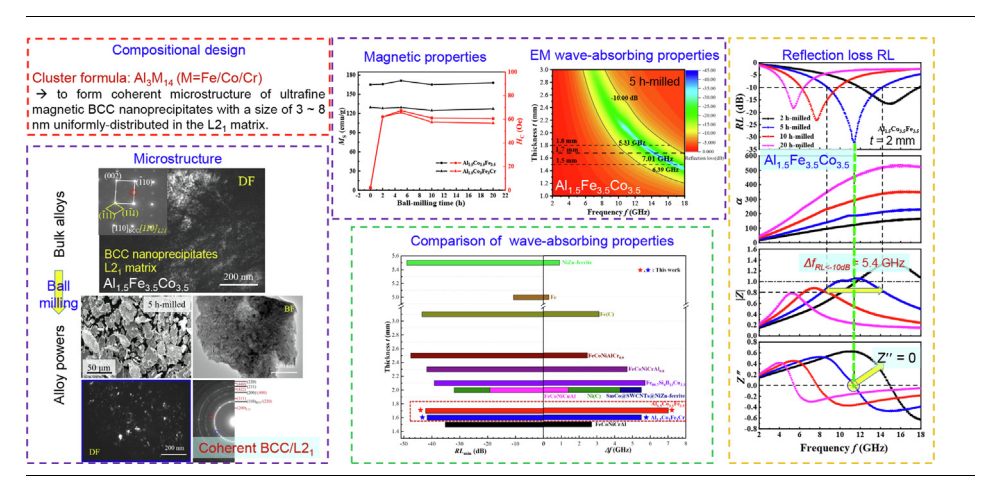
- The prominent soft magnetic properties are ascribed to their special coherent microstructure.
- A short-time ball-milling does not change the coherent BCC/ L2₁ structure of MEA powders.
- The prominent soft magnetic and high resistivity, which contributes to the excellent electromagnetic waveabsorbing properties.
- Al_{1.5}Co_{3.5}Fe_{3.5} flake powders possess the maximum effective bandwidth of 7.01 GHz with a sample thickness of 1.7 mm

ARTICLE INFO

Article history: Received 20 May 2022 Revised 3 August 2022 Accepted 8 August 2022 Available online 11 August 2022

Keywords: Medium-entropy alloys Coherent precipitation Soft-magnetic property Electromagnetic property

G R A P H I C A L A B S T R A C T



ABSTRACT

Magnetic alloy powders show a great superiority in the balance of permittivity and permeability for electromagnetic (EM) wave-absorption. However, it is necessary to enhance their effective absorption bandwidth (Δf) and impedance matching due to their insufficient soft-magnetic properties and low resistivity, which would be solved by high/medium-entropy alloys (HEAs/MEAs). In this report, we designed Al_{1.5}Co_{3.5}Fe_{3.5} and Al_{1.5}Co₃Fe₃Cr MEAs with prominent soft-magnetic property and high resistivity. It is contributed to the special coherent microstructure with ultrafine magnetic body-centered-cubic nanoprecipitates uniformly-distributed into the L2₁ matrix, which could not be changed by ball-milling. Thus, alloy powders possess excellent EM properties, as evidenced by the minimum reflection loss of -42.2 dB at 14.52 GHz and the largest $\Delta f = 7.01$ GHz in 5 h-milled Al_{1.5}Co_{3.5}Fe_{3.5}, better than existing alloy powders. The wave-absorbing behavior of MEA powders was discussed from both permittivity and permeability. The current findings offer a useful design strategy for developing high-performance absorbers.

© 2022 The Authors. Published by Elsevier Ltd. This is an open access article under the CC BY-NC-ND license (http://creativecommons.org/licenses/by-nc-nd/4.0/).

1. Introduction

Electromagnetic (EM) wave-absorbing materials, mainly including dielectric and magnetic materials, have attracted more

E-mail addresses: wangq@dlut.edu.cn (Q. Wang), duanyp@dlut.edu.cn (Y. Duan).

^b Department of Materials Science and Engineering, The University of Tennessee, Knoxville 37996, TN, USA

^{*} Corresponding authors.

attention due to their higher efficiency for absorbing EM waves and transforming them into other energies [1-4]. High absorption intensity and wide effective absorption bandwidth are necessary for good absorbing materials, which are controlled by two characteristic parameters, complex permittivity ($\varepsilon = \varepsilon' - j\varepsilon''$) and complex permeability ($\mu = \mu' - j\mu''$) that determine both the loss capability and impedance matching [3]. Among these materials, magnetic alloy powders have prominent magnetic-loss abilities, showing a great advantage in the balance of ε and μ [2,5–7]. The loss mechanism is mainly related to the magnetic loss, in which a high μ , especially a high imaginary permeability (μ ") corresponds to a large magnetic energy dissipation, and a comparable ε could contribute to an optimum impedance matching [7]. It is emphasized that the μ is primarily correlated to the soft-magnetic properties (high saturation magnetization M_S and low coercivity H_C) of materials, while the ε is inversely proportional to the electrical resistivity ρ [8–10]. For instance, conventional ferrite magnetic materials have good impedance matching due to their high resistivity $(\rho = 10^2 \sim 10^8 \ \Omega \cdot \text{cm})$, being widely used in a low-frequency microwave band (f < 1 GHz)[11-14]. However, its permeability was limited by the Snoek law induced by the lower saturation magnetization ($M_S = 20 \sim 80 \text{ emu/g}$), leading to a poor loss capacity in high-frequency range [11]. By contrast, magnetic alloy powders containing Fe, Co, and Ni elements have relatively higher both $M_{\rm S}$ (130 \sim 190 emu/g) and μ , which are often used in the highfrequency $C \sim Ku$ bands ($f = 4 \sim 18$ GHz) [2,5–7]. But their lower resistivity (ρ = 40 \sim 50 $\mu\Omega\cdot$ cm) worsens the impedance matching, resulting in a narrower effective absorption bandwidth [15]. It was reported that the effective absorption bandwidth of Fe₇₅Si₉Al₁₄ flaky powers is only $\Delta f_{RL<-10dB}$ = 0.71 GHz (f = 3.82 \sim 4.53 GHz with the reflection loss RL less than -10 dB) at the sample thickness being t = 2 mm, although it has a high $M_S = 134$ emu/g and a high $\mu' = 2.34$ at 2 GHz [6]. In addition, Fe-based amorphousnanocrystalline alloy powders exhibit good EM wave-absorbing properties due to their high $M_{\rm S}$ (71 \sim 182 emu/g), low $H_{\rm C}$ (\sim 30 Oe), and high ρ (~115 $\mu\Omega$ ·cm), as evidenced by the fact that the effective absorption bandwidth of $Fe_{80.7}Si_4B_{13}Cu_{2.3}$ spherical powers could reach up to $\Delta f_{RL<-10dB}$ = 5.7 GHz (9 \sim 14.7 GHz) at t = 2.1 mm [16,17]. However, the metastable amorphous matrix is apt to transform into a crystalline state, leading to a deterioration of EM wave-absorption [18,19]. Therefore, a synergistic combination of high ρ , high M_S , and high μ induced by low H_C would contribute to an optimum integration of impedance matching and loss ability for EM wave-absorbing materials.

More recently, a special kind of newly-developed magnetic high-entropy and medium-entropy alloys (HEAs or MEAs), consisting of multi-principal elements, show great potential in electromagnetic applications since they have excellent soft-magnetic properties (high M_S and low H_C), as well as high resistivity ρ [10,15,20-24]. These HEAs/MEAs are mainly based on Fe, Co, and Ni, as evidenced by the fact that the effective absorption bandwidth of FeCoNiAlCr_{0.9} flake alloy powders synthesized by mechanical alloying could reach up to $\Delta f_{RL<-10dB}$ = 4.28 GHz (9.3 \sim 13.58 GHz) with t = 2 mm, in which the maximum reflection loss is down to RL = -29.72 dB at 11.2 GHz [20]. Moreover, these alloys also exhibit good corrosion and oxidation resistances at high temperatures due to the addition of Cr and Al elements [25,26]. Unfortunately, the saturation magnetization of existing magnetic HEA/ MEA powders is slightly lower and the coercivity is relatively higher, being M_S < 80 emu/g and H_C > 100 Oe, which needs to be improved further for a much higher μ .

In previous works, we obtained a series of soft-magnetic MEAs in Al-Co-Fe-Cr system via the cluster composition formula of Al₃M₁₄ (M being different combinations of Fe, Co, and Cr), as evidenced by the fact that the designed Al₃Co₈Fe₄Cr₂ (=Al_{1.5}Co₄Fe₂Cr) MEA exhibits prominent soft-magnetic property with a higher

 M_S = 135.3 emu/g, lower H_C = 1.6 Oe, and higher Curie temperature $(T_C = 1061 \text{ K})$ [15]. It is primarily ascribed to its coherent microstructure of ultrafine ferromagnetic body-centered-cubic (BCC) nanoprecipitates with a size of 3 ~ 7 nm uniformlydistributed into a B2 matrix [15]. Moreover, these MEAs have a much greater resistivity of $\rho \sim 250 \ \mu\Omega$ cm due to the chaos effect caused by the multi-principal elements. Therefore, the present work will aim at investigating the EM wave-absorbing behavior of Al₃M₁₄ soft-magnetic MEAs, in which two typical alloys are selected, the Cr-free Al_{1.5}Co_{3.5}Fe_{3.5} (Al₃Co₇Fe₇) and the Crcontaining Al_{1.5}Co₃Fe₃Cr (Al₃Co₆Fe₆Cr₂). The magnetic properties of alloy bulks and powders are measured firstly to compare the difference between them. Then, the EM wave-absorbing properties of alloy powders are characterized, in which the influences of alloy composition, morphology of powder particles, and magnetic property on the EM wave-absorbing behavior are discussed.

2. Material and methods

2.1. Alloy fabrication

Alloy ingots with a nominal composition of $Al_{1.5}Co_{3.5}Fe_{3.5}$ and $Al_{1.5}Co_3Fe_3Cr$ (at %) were prepared by means of arc melting under an argon atmosphere, in which the purity of each raw metal is 99.99 wt%. The ingots with a weight of about 20 g were remelted at least five times to ensure the chemical homogeneity. Then they were homogenized in a muffle furnace at 1573 K for 2 h, and aged at 773 K for 24 h, in which each step was followed by water quenching. The aged alloy ingots were crushed and sieved to obtain powders with the particle size less than 250 μ m, and subsequently wet-milled by a planetary ball mill with a rotation speed of 350 rpm, in which the anhydrous ethanol was used as process-control agent. Stainless steel pots with a capacity of 250 mL and balls with diameters of 10 mm and 6 mm were used, and the mass ratio of balls to powders was 30:1. The milling time were taken as 2, 5, 10, and 20 h, respectively.

2.2. Characterization

The crystalline structure and microstructural morphology of alloy samples in different states were identified using the Bruker D8 X-ray diffractometer (XRD, Cu K_{α} radiation, λ = 0.15406 nm), the Olympus optical microscopy (OM), Zeiss Supra 55 scanning electron microscope (SEM), and the JEOL-JEM-2100F field emission transmission electron microscopy (TEM), respectively. Image analysis of the microstructural details were made in the ImageJ software [27]. Statistical analysis on the size of flaky particles and BCC nanoprecipitates was performed with at least 6 SEM and TEM morphology images, respectively. The particle size of flaky powders was obtained from over 150 particles, and determined with a circle-equivalent diameter (i.e., D_p = (length + width)/2).

2.3. Property testing

The saturation magnetization $M_{\rm S}$ and coercivity $H_{\rm C}$ were measured with a vibrating sample magnetometer (VSM, Lake Shore 7410) under a maximum applied field of 15,000 Oe, in which the sample size of bulk alloys was $3.0 \times 2.0 \times 1.0$ mm (length \times width \times thickness), and the demagnetization was carried on before the measurement. The resistivity was tested with a fourpoint probe measurement tool (RTS-9), and the resulting cylinders were pressed using powders at 10 MPa. The electromagnetic parameters of permittivity and permeability in a frequency range of $2 \sim 18$ GHz were measured by a vector network analyzer (8720B, Agilent) using a coaxial reflection/transmission method,

in which the toroidal samples with a size of 2.0~mm (thickness) \times 3.0~mm (inner diameter) \times 7.0~mm (outer diameter) were made by homogeneously mixed powders and paraffin composites with a mass ratio of 3:2.

3. Results

3.1. Microstructural characterization of alloy bulks and powders

The XRD patterns of $Al_{1.5}Co_{3.5}Fe_{3.5}$ and $Al_{1.5}Co_3Fe_3Cr$ alloy bulks and powders after 20 h-milling (Fig. S1) show that the bulk alloys consist of BCC-related phases and the ball-milling does not change the crystalline structure of alloys. Actually, there exists weak diffraction peaks of (111) and (200) planes of ordered $L2_1$ phase (cF-Fe₃Al type), which would be identified obviously by the TEM analysis. The microstructure of bulk alloys is constituted of equiaxed grains (Fig. 1a). And the TEM dark-filed (DF) image and

selected-area electron diffraction (SAED) pattern along the $[110]_{BCC}$ direction in Fig. 1b indicate that the crystalline structure is indeed composed of BCC and L2₁ phases, in which the L2₁ with a Fe₃Al structure is a highly-ordered coherent phase of the BCC solid solution. More importantly, the ultrafine BCC nanoprecipitates with a size of about $3 \sim 8$ nm are uniformly distributed into the L2₁ matrix. Although the ball-milling weakens the diffraction peaks induced by the superlattice in XRD patterns, the TEM-SAED patterns for these two alloy powders (Fig. 1f, j) show that the distinct diffraction rings (like (311), (422), and (440)) of ordered L2₁ phase co-exist with those of the BCC phase. In addition, the crystalline structures of alloy powders are not changed with the ball-milling time, being constituted of nanocrystals of both BCC and L2₁ phases with a size of about $8 \sim 15$ nm due to a serious deformation caused by ball-milling, as seen in the TEM bright-field (BF) and DF images (Fig. 1c, e, g, i) for Al_{1.5}Co_{3.5}Fe_{3.5} powder after 5 h-milling and Al_{1.5}Co₃Fe₃Cr powder after 10 h-milling.

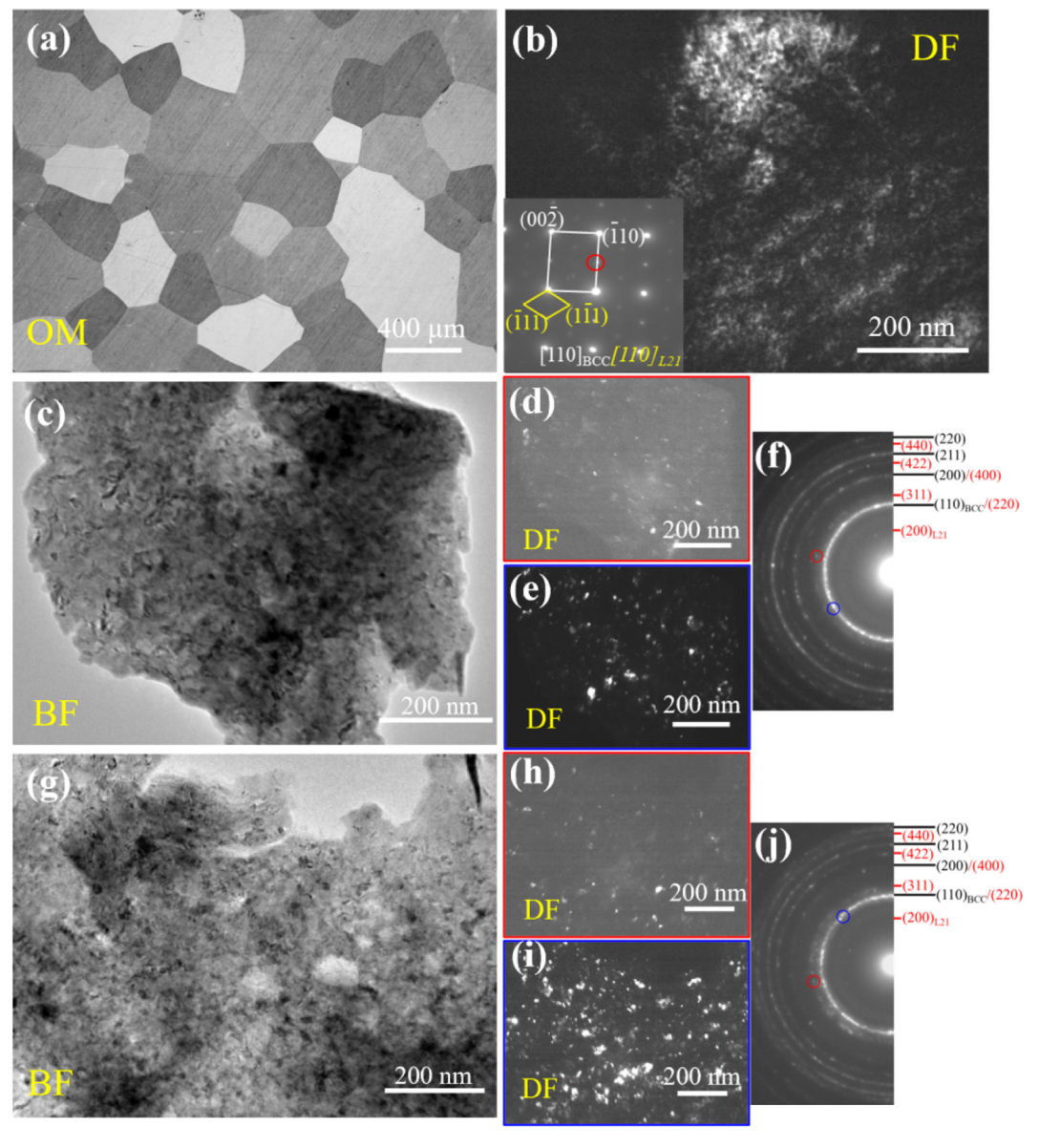


Fig. 1. OM and TEM observations of $Al_{1.5}Co_{3.5}Fe_{3.5}$ and $Al_{1.5}Co_{3}Fe_{3}Cr$ MEA bulks and powders. (**a and b**) $Al_{1.5}Co_{3.5}Fe_{3.5}$ bulk alloy, in which the TEM dark-field (DF) and the corresponding selected-area electron diffraction (SAED) pattern indicate that ultrafine BCC nanoprecipitates with a size of about $3 \sim 8$ nm are uniformly distributed into the $L2_1$ matrix. (**c** \sim **f**) $Al_{1.5}Co_{3.5}Fe_{3.5}$ alloy powder after ball-milling for 5 h, in which both TEM bright-field (BF) and DF images and the SEAD pattern indicate the co-existence of BCC and $L2_1$ nanocrystals with a size of $8 \sim 15$ nm; (**g** \sim **j**) $Al_{1.5}Co_{3.5}Fe_{3.5}$ power.

The particle morphologies of Al_{1.5}Co_{3.5}Fe_{3.5} and Al_{1.5}Co₃Fe₃Cr alloy powders with the milling time are shown in Fig. 2 and Fig. S2. All alloy powders in different milled states present a flaky particle feature, which is ascribed to the flattening effect of the process-control agent [6]. We counted the average particle size (D_n) and the aspect ratio (δ) of the particle diameter to thickness of these two alloy powders in different milled states, and the statistic values are presented in Fig. 3. It is found that the average particle size of alloy powders increases slightly with the milling time from 2 h to 20 h, being in a range of D_p = 20 \sim 30 μ m. While the aspect ratio is strongly affected by the milling time, especially in Al_{1.5}Co_{3.5}Fe_{3.5}, showing a sharp increase from δ = 2.8 in 2 hmilled state to δ = 20.7 in 20 h-milled state. Similar tendency also appears in Al_{1.5}Co₃Fe₃Cr. In general, the Al_{1.5}Co₃Fe₃Cr alloy powders possess relatively-smaller particle size and aspect ratio than the Al_{1.5}Co_{3.5}Fe_{3.5} in the same milled state, which might result from the alloy brittleness due to the addition of Cr [28].

3.2. Magnetic properties

The hysteresis loops of $Al_{1.5}Co_{3.5}Fe_{3.5}$ and $Al_{1.5}Co_{3}Fe_{3}Cr$ alloy bulks and powders were measured at room temperature with an applied field from -15000 Oe to 15,000 Oe, as presented in Fig. 4. It can be seen that these two bulk alloys possess prominent

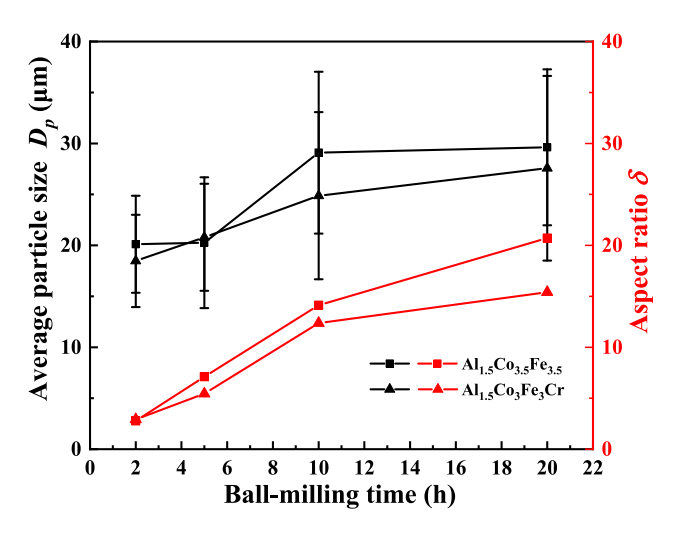


Fig. 3. Variations of the average particle size D_p and the aspect ratio δ of particle diameter to thickness with the ball-milling time in Al_{1.5}Co_{3.5}Fe_{3.5} and Al_{1.5}Co₃Fe₃Cr alloy powders.

soft-magnetic properties with lower coercivity (H_C = 1.9 \sim 2.3 Oe) and higher saturation magnetization (M_S = 165.2 emu/g for Al_{1.5}Co_{3.5}Fe_{3.5} and M_S = 129.6 emu/g for Al_{1.5}Co₃Fe₃Cr). The much

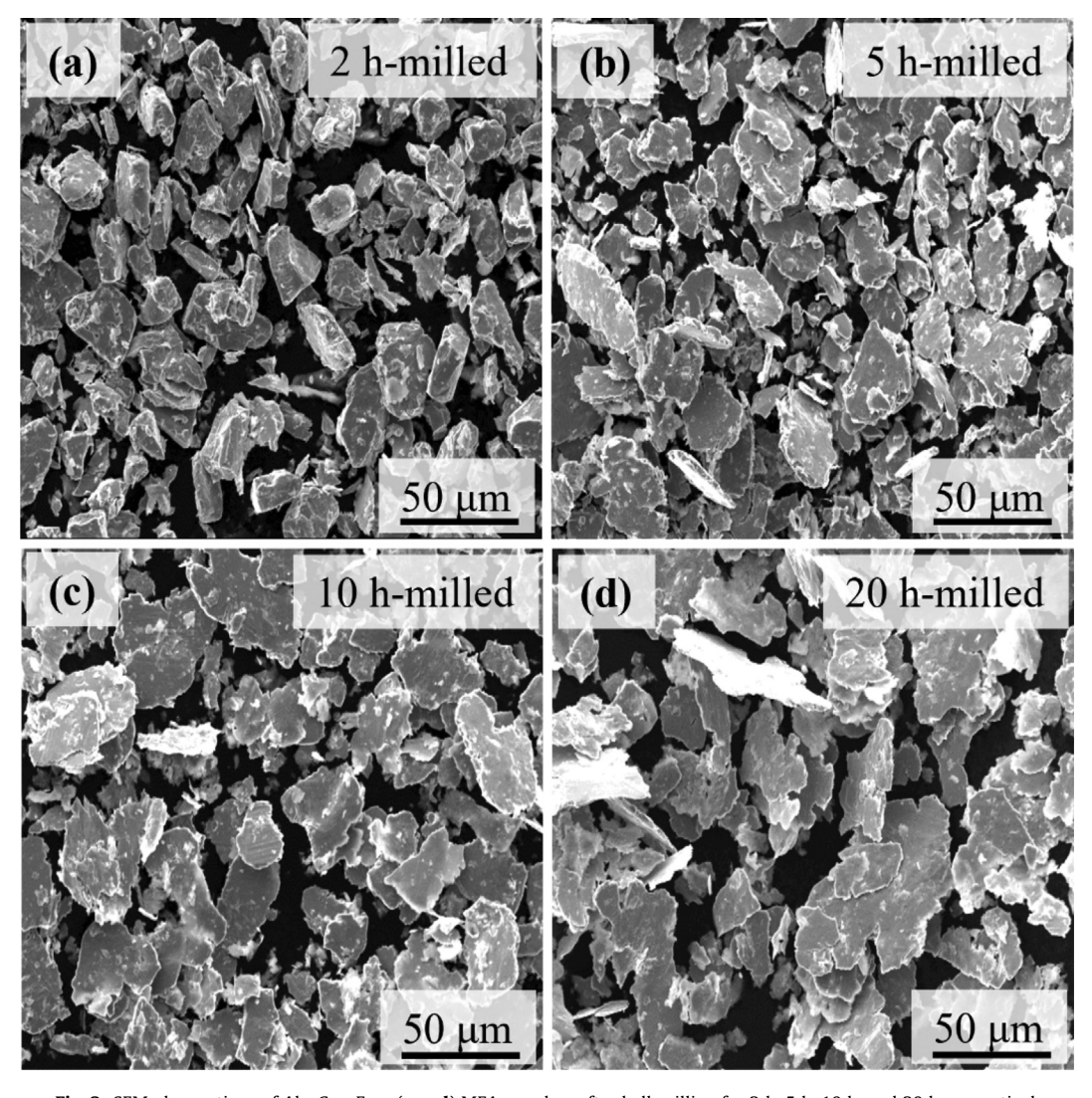


Fig. 2. SEM observations of Al $_{1.5}$ Co $_{3.5}$ Fe $_{3.5}$ (a \sim d) MEA powders after ball-milling for 2 h, 5 h, 10 h, and 20 h, respectively.

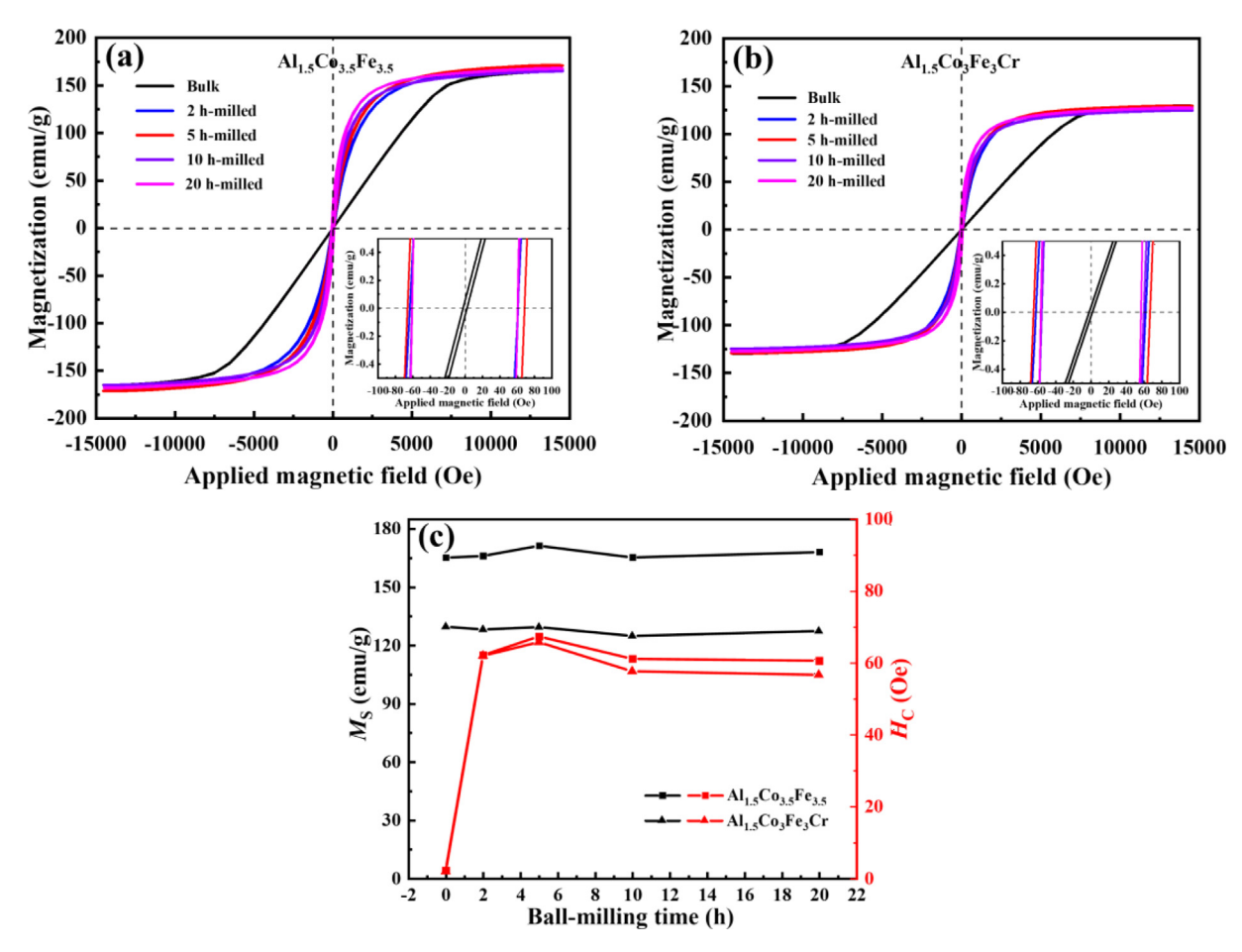


Fig. 4. Hysteresis loops of $Al_{1.5}Co_{3.5}Fe_{3.5}$ (**a**) and $Al_{1.5}Co_3Fe_3Cr$ (**b**) alloy bulks and powders with different milling time, in which the variations of both M_S and H_C with the milling time are shown in (**c**).

higher $M_{\rm S}$ in the former alloy might be ascribed to the relatively high amount of magnetic elements of Fe and Co since both have similar BCC/L2₁ coherent microstructure, which is well consistent with previous results [15]. Fig. 4c gives the variations of both $M_{\rm S}$ and $H_{\rm C}$ with the milling time, where the $M_{\rm S}$ values of alloy powers keep constant with the milling time, as evidenced by $M_{\rm S}$ = 165.3 \sim 171.4 emu/g for Al_{1.5}Co_{3.5}Fe_{3.5} and $M_{\rm S}$ = 124.8 \sim 129.4 emu/g for Al_{1.5}Co₃Fe₃Cr, being comparable to their corresponding bulk samples. However, the coercivity is enhanced drastically up to a higher level with $H_{\rm C}$ = 56 \sim 68 Oe by the ball milling, and it is not affected by the short milling time.

3.3. Electromagnetic properties

The characteristic parameters of the permittivity ε and permeability μ , representing electromagnetic properties of Al_{1.5}Co_{3.5}Fe_{3.5} and Al_{1.5}Co₃Fe₃Cr powders in different milled states were investigated, and the variations in the frequency range of 2 \sim 18 GHz are shown in Fig. 5 and Fig. S3. Among them, the real parts (ε ' and μ ') of the permittivity and permeability are associated with the storage capabilities of electric and magnetic energies, respectively, and their imaginary parts (ε " and μ ") are related to the dissipation capacities. It is found that the ε ' values of both these two alloy powders increase gradually with the milling time (Fig. 5a and Fig. S3a), and the ε ' in each state keeps almost constant within the whole frequency range. While the ε " values of these powders after a short-time milling (<10 h) are all close to zero in the whole frequency range (Fig. 5b and Fig. S3b), indicating no dielectric loss. The exception appears in those powders after a relatively long-

time milling, such as the 10 h-milled $Al_{1.5}Co_{3.5}Fe_{3.5}$ and 20 h-milled $Al_{1.5}Co_3Fe_3Cr$, where the ϵ " is less than zero in a high frequency range.

For the permeability, both the μ' and μ'' of these two alloy powders are increasing with the ball-milling time. Moreover, the variation of μ' for alloy powders in a specific milled state would decrease with the increase of frequency (Fig. 5c and Fig. S3c). While for the μ'' , there exist two typical resonance peaks in these two alloy powders at 5 \sim 7 GHz and 11 \sim 13 GHz, respectively, which is particularly noticeable in Al_{1.5}Co_{3.5}Fe_{3.5} (Fig. 5d and Fig. S3d). Actually, the resonance peaks at 5 \sim 7 GHz and at 11 \sim 13 GHz correspond to the natural resonance and exchange resonance, respectively, since the natural resonance generally occurs at a high frequency band of 0.1 \sim 10 GHz, while the exchange resonance appears at an extremely-high frequency band (>10 GHz) [10].

3.4. Electrical properties

The electrical properties of $Al_{1.5}Co_{3.5}Fe_{3.5}$ and $Al_{1.5}Co_3Fe_3Cr$ alloy powders in different milled states were measured at room temperature. Fig. 6 gives the variations of electrical conductivity (σ) and electrical resistivity (ρ) of these two alloy powders with the ball-milling time, from which it could be seen that the conductivity decreases with increasing the milling time. It means that the milling time increases the electrical resistivity of alloy powders. In addition, the $Al_{1.5}Co_3Fe_3Cr$ powders possess a much lower conductivity than the $Al_{1.5}Co_3.5Fe_{3.5}$, indicating that the former has a much higher resistivity $(\rho = 2.26 \sim 21.85 \text{ m}\Omega \cdot \text{cm})$. It might be ascribed to

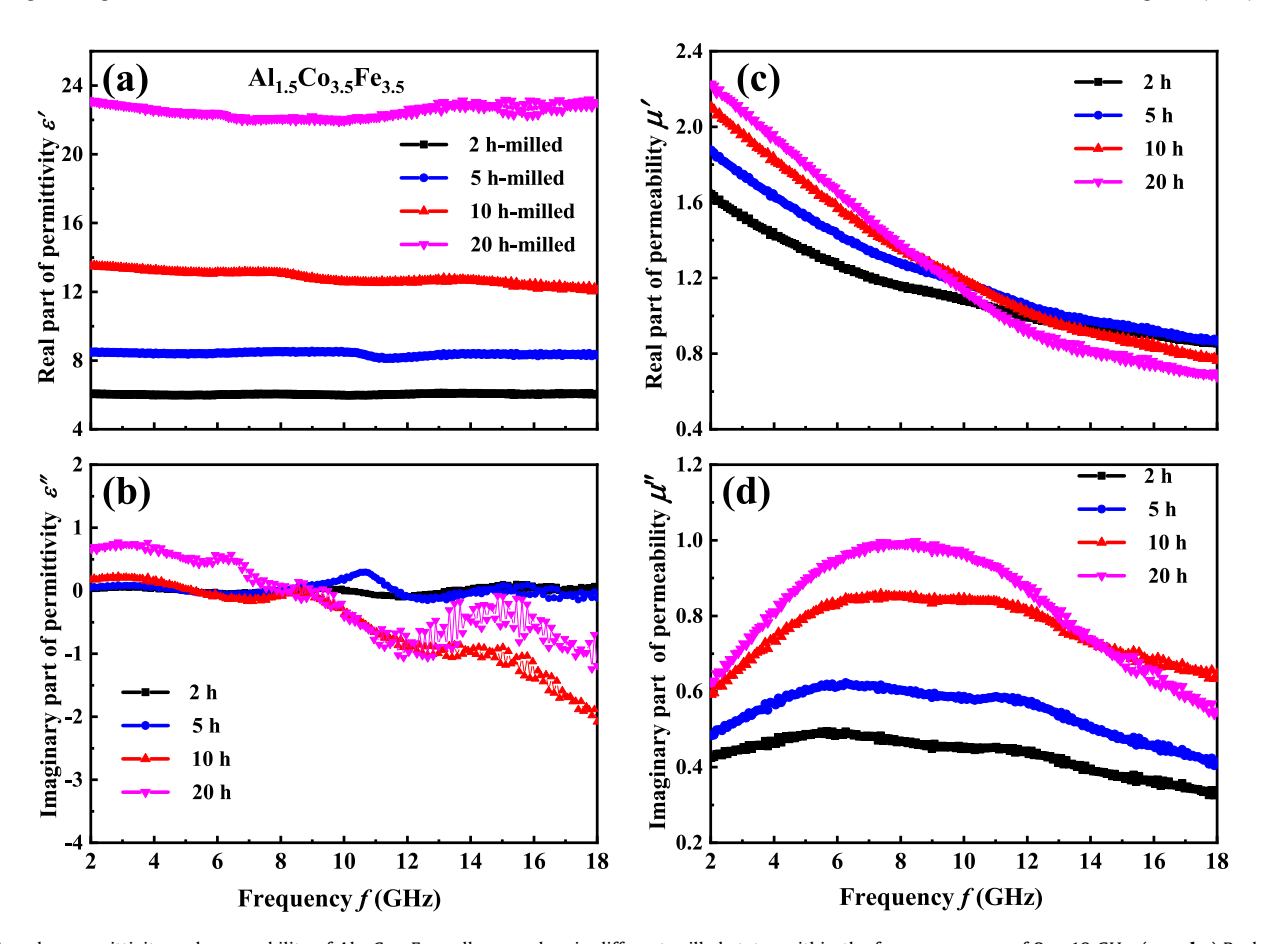


Fig. 5. Complex permittivity and permeability of Al_{1.5}Co_{3.5}Fe_{3.5} alloy powders in different milled states within the frequency range of $2 \sim 18$ GHz. (**a and c**) Real part of permittivity ϵ ' and permeability μ '; and (**b and d**) Imaginary part of permittivity ϵ " and permeability μ ".

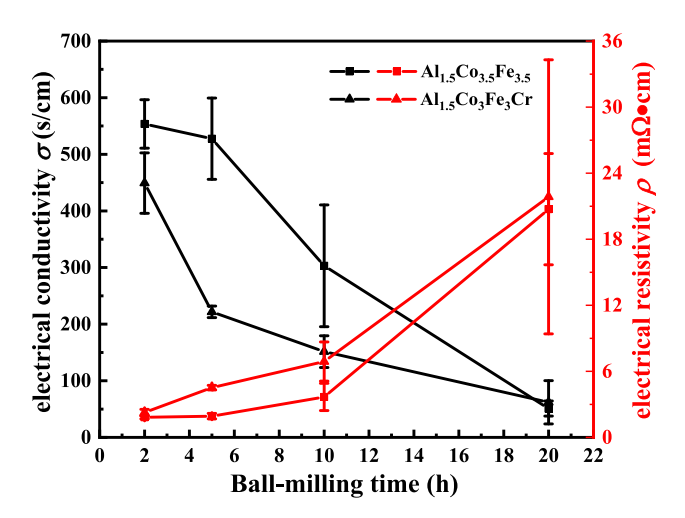


Fig. 6. Variations of the electrical conductivity σ and resistivity ρ of Al_{1.5}Co_{3.5}Fe_{3.5} and Al_{1.5}Co₃Fe₃Cr alloy powders with the ball-milling time.

that the addition of Cr element induces a larger confusion of atomic packing, i.e., a high-entropy effect [29–31].

4. Discussion

4.1. Magnetic properties of alloy bulks and powders

From the variations of the saturation magnetization M_S and the coercivity H_C of $Al_{1.5}Co_{3.5}Fe_{3.5}$ and $Al_{1.5}Co_3Fe_3Cr$ alloy powders

with the milling time in Fig. 4c, it could be found that the M_S of Al_{1.5}Co_{3.5}Fe_{3.5} is obviously higher than that of Al_{1.5}Co₃Fe₃Cr in the same milled state, while the H_C values of these two alloy powders in different milled states are all comparable. Generally speaking, the M_S of an alloy is primarily controlled by the amount of ferromagnetic elements (Fe, Co, and Ni) and the crystalline structure, in which the BCC-related structure is more favorable than the face-centered-cubic (FCC) structure to improve M_S [32]. Thus, the M_S of Al_{1.5}Co_{3.5}Fe_{3.5} alloy is higher than that of Al_{1.5}Co₃Fe₃Cr because the anti-ferromagnetic Cr element substitutes for ferromagnetic elements of Co and Fe in the latter alloy under the case that both have the same $BCC/L2_1$ phase structure. For the H_C , it is known that any crystalline defects in alloys that block the movement of magnetic domain walls would lead to an increase in H_c . Generally, the H_C is strongly related to the grain size of alloy matrix or to the particle size of nanoprecipitates [8,33,34], in which a relatively large grain size (>100 µm) or an ultrafine particle size of nanoprecipitates (< 20 nm) would contribute to an extremelylow coercivity with H_C < 0.5 Oe [34], as a result of a prominent soft-magnetic property. Only when the grain size or the particle size is within the range of 0.1 \sim 10 μ m, the H_C would be enhanced up to a high level, leading to the deterioration of soft-magnetic property. Thus, it could be deduced that the ultrafine nanoprecipitates (8 \sim 15 nm) and the coarser flaky particles (20 \sim 30 um) of the current alloy powders would contribute to a lower coercivity with H_C < 0.5 Oe. However, it is contradictory to the measured value of H_C = 56 \sim 68 Oe. Therefore, the relatively high coercivity of the current alloy powders should be mainly ascribed to the large amount of defects and internal stresses generated during the ball milling process, which has been demonstrated in many existing works [10,15,20-24].

4.2. Effects of magnetic property and particle morphology of alloy powders on electromagnetic parameters

According to the variations of permittivity and permeability of Al_{1.5}Co_{3.5}Fe_{3.5} and Al_{1.5}Co₃Fe₃Cr alloy powders with the frequency and milling time (Fig. 5 and Fig. S3), although the real part ε ' of permittivity is hardly affected by the frequency and keeps almost constant, it increases with the milling time. It has been reported that the ε ' is closely related to the polarization and conductivity of alloy powders. With prolonging the milling time, the aspect ratio of powder particles increases obviously (Fig. 3), where a larger aspect ratio could result in a much more enhanced surface polarization and then induce a higher ε' [6]. On the other side, the ε' is also proportional to the conductivity σ in light of the Debye's relaxation theory [10], thus, a lower σ (or a higher resistivity ρ) would lead to a lower ε '. Therefore, the increase of ε ' with the milling time of alloy powders might be mainly ascribed to the increase of the aspect ratio, on the premise that the conductivity decreases with the increase of the milling time. In the same milled state, the Al_{1.5}- $Co_{3.5}Fe_{3.5}$ powder exhibits a relatively-higher ε ' than $Al_{1.5}Co_{3}Fe_{3}Cr$, which is due to that the former has both a larger aspect ratio of powder particles and a higher conductivity, as presented in Fig. 3 and Fig. 6.

For the real part μ ' of permeability, it is approximately equal to the initial permeability μ_i , which could be expressed with Eq. (1): [8].

$$\mu' \sim \mu_i = \frac{p_c p_\mu M_s}{H_c} \tag{1}$$

where p_c and p_μ are dimensionless pre-factors of the order of unity. It could be found that the μ_i is directly proportional to the M_S and inversely proportional to the H_C , indicating that a higher M_S and a lower H_C would lead to a high μ_i and μ' . Although these two current alloy powders in different milled states have comparable H_C value (56 \sim 68 Oe), the Al_{1.5}Co_{3.5}Fe_{3.5} powders have a much higher M_S (165.3 \sim 171.4 emu/g) than Al_{1.5}Co₃Fe₃Cr (M_S = 124.8 \sim 129.4 emu/g), which inevitably yields a higher μ' in the former.

More importantly, it needs to be emphasized that the μ_i of magnetic powders is limited by the classical shape-dependent Snoek's law, as expressed with Eq. (2): [35].

$$\mu_i - 1 = 4\pi M_s / (H_k + 4\pi M_s N_h) \tag{2}$$

$$N_h = (1 - N_\perp)/2 \tag{2a}$$

$$N_{\perp} = \frac{\delta^2}{\delta^2 - 1} \times (1 - \sqrt{\frac{1}{\delta^2 - 1}} \times \arcsin{\frac{\sqrt{\delta^2 - 1}}{\delta}})$$
 (2b)

where H_k is the magneto-crystalline anisotropy energy; N_h and N_\perp are the demagnetization factors in the direction of the particle diameter and thickness, respectively; and δ is the aspect ratio of flake powders. It is found that besides the $M_{\rm S}$, a high μ_i could also be achieved by decreasing H_k and N_h , in which the H_k is mainly related to the microstructure and the N_h is dependent on the shape anisotropy of magnetic powder particles. Generally, flaky particles with a larger aspect ratio would induce a remarkable shape anisotropy, resulting in a smaller N_h [36], while the H_k is constant when fixing the microstructure [35]. For the two present alloy powders, the aspect ratio gradually increases with the ball-milling time, but the microstructure does not change during the ball-milling process, which certainly results in a reduction of N_h and then enhances the μ_i and μ' , even the microstructure-related H_k is not unchanged.

For the imaginary part μ " of the permeability, both Al_{1.5}Co_{3.5}-Fe_{3.5} and Al_{1.5}Co₃Fe₃Cr alloy powders present a downward parabola-shape with the frequency (Fig. 5d and Fig. S3d), and the variation tendency of μ " with the ball-milling time is similar to

that of μ '. Actually, it could be well interpreted from the eddy current loss, as expressed with Eq. (3): [7].

$$\mu'' = 2\pi \mu_0(\mu)^2 t^2 f \sigma / 3 \tag{3}$$

where μ_0 is the vacuum permeability, t is the sample thickness, f is the frequency of incident electromagnetic wave, and σ is the electrical conductivity. It can be found that the μ " has a positive correlation to both the σ and the square of μ '.

4.3. Influence of electromagnetic parameters on reflection loss

The coaxial-line method was used to calculate the reflection loss (*RL*) of the milled alloy powders/paraffin composites. It is one of the most important parameters to characterize the EM wave-absorption performance, which could be expressed with the Eq. (4): [37].

$$RL(dB) = 20log \left| \frac{Z_{in} - Z_0}{Z_{in} + Z_0} \right|$$
 (4)

$$Z_{in} = Z_0 \left(\frac{\mu}{\varepsilon}\right)^{\frac{1}{2}} \tanh \left[j \left(\frac{2\pi f t}{c}\right) (\mu \varepsilon)^{\frac{1}{2}} \right]$$
 (4a)

where Z_{in} is the impedance of materials, Z_0 is the intrinsic impedance in a free space, c is the light velocity, and μ and ε are complex permeability and permittivity, respectively. Since both Z_{in} and Z_0 are positive real numbers, the calculated RL must be negative. Hence, the higher the absolute value of RL, the better the waveabsorption performance at a given frequency. When the RL is less than - 10 dB, it means that 90 % of incident electromagnetic waves can be absorbed, in which the involved frequency band is usually determined as the effective absorption bandwidth (Δf). The variations of RL of the alloy powders/paraffin composites with the frequency at a sample thickness of t = 2 mm for $Al_{1.5}Co_{3.5}Fe_{3.5}$ and Al_{1.5}Co₃Fe₃Cr in different milled states are shown in Fig. 7 (a and e). Distinctly, the RL values of alloy powders decrease firstly with the milling time, and then increase gradually. Among them, the 5 h-milled Al_{1.5}Co_{3.5}Fe_{3.5} and 10 h-milled Al_{1.5}Co₃Fe₃Cr exhibit the optimal reflection loss, as evidenced by the fact that the minimum *RL* and the effective absorption bandwidth are $RL_{min} = -32.1$ dB and Δf = 5.4 GHz (8.77 \sim 14.17 GHz) for the former, and RL_{min} = -30.0 dB and $\Delta f = 4.5$ GHz (8.17 ~ 12.67 GHz) for the latter, respectively.

Actually, the *RL* is mainly attributed to both the impedance matching |Z| ($|Z| = |Z_{in}/Z_0|$) and the microwave attenuation α expressed with Eq. (5) [14].

$$\alpha = \frac{\sqrt{2}\pi f}{c}\sqrt{\mu''\epsilon'' - \mu'\epsilon' + \sqrt{\left(\mu''\epsilon'' - \mu'\epsilon'\right)^2 + \left(\mu'\epsilon'' + \mu''\epsilon'\right)^2}} \tag{5}$$

Fig. 7b and f give the variations of α with the frequency and the ball-milling time, in which a larger α can effectively consume electromagnetic waves and reduce transmission. Obviously, the α increases with the milling time, however, the largest α in 20 h-milled state does not correspond to the minimum RL. The variations of the impedance matching |Z| with the frequency are presented in Fig. 7c and 7 g, in which the value of $|Z| \sim 1.0$ corresponds to the optimum impedance matching and the electromagnetic waves can enter into the materials completely without any reflection. Moreover, it is found that in the effective absorption bandwidth with RL < -10 dB for the 5 h-milled Al_{1.5}Co_{3.5}Fe_{3.5} and 10 h-milled Al_{1.5}Co₃Fe₃Cr, the |Z| values are close to 1.0. Especially, the RL_{min} corresponds to the value of Z'' = 0, in which Z'' is the imaginary of the impedance matching Z, as seen in Fig. 7 (d and h). In

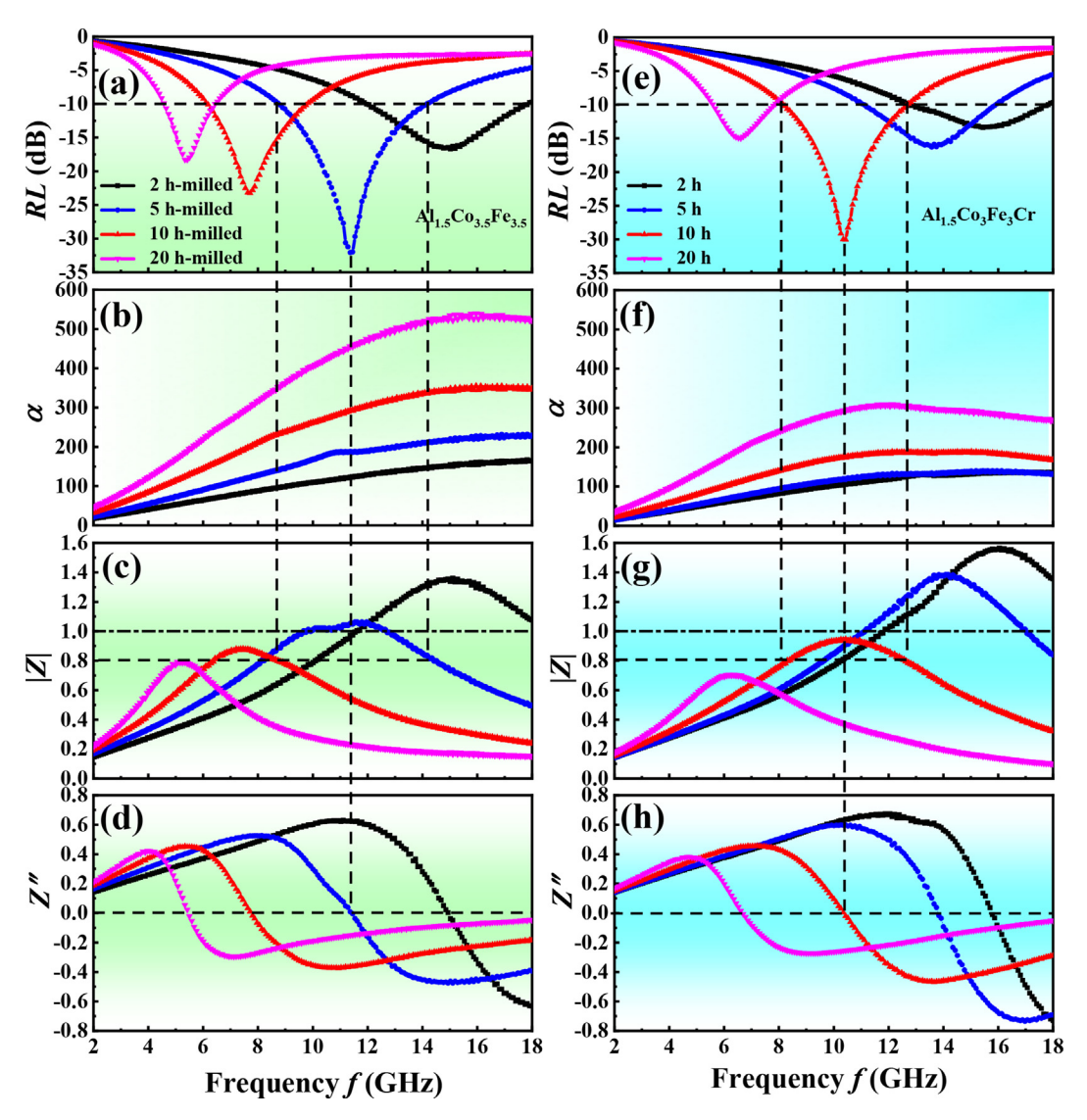


Fig. 7. Variations of the reflection loss RL, microwave attenuation α , impedance matching |Z| and Z'' with the frequency of $Al_{1.5}Co_{3.5}Fe_{3.5}$ ($\mathbf{a} \sim \mathbf{d}$) and $Al_{1.5}Co_3Fe_3Cr$ ($\mathbf{e} \sim \mathbf{h}$) alloy powders in different milled states with a thickness of 2 mm.

addition, the RL_{min} of 5 h-milled $Al_{1.5}Co_{3.5}Fe_{3.5}$ is slightly smaller than that of 10 h-milled $Al_{1.5}Co_{3}Fe_{3}Cr$, which is mainly due to that the microwave attenuation α is relatively larger and the impedance matching |Z| is much closer to 1.0.

As expressed in Eq. (4), the EM wave-absorption property is also related to the sample thickness t of absorbing materials. The relationship between the RL with the sample thickness and the frequency for both 5 h-milled Al_{1.5}Co_{3.5}Fe_{3.5} and 10 h-milled Al_{1.5}Co₃Fe₃Cr alloy powders were calculated and shown in Fig. 8 and Fig. S4. For the 5 h-milled Al_{1.5}Co_{3.5}Fe_{3.5}, the minimum RL could reach down to $-35 \sim -42$ dB with the sample thickness being $t = 1.5 \sim 1.8$ mm, and the effective absorption bandwidth is Δf = 5.31 \sim 7.01 GHz (9.88 \sim 18.0 GHz). Especially at t = 1.7 mm, the minimum RL reaches -42.2 dB at f = 14.52 GHz, and the effective absorption bandwidth of 7.01 GHz (10.99 \sim 18 G Hz) can cover the Ku-band (12 \sim 18 GHz) completely. For the 10 hmilled $Al_{1.5}Co_3Fe_3Cr$ with t = 1.6 mm, the minimum RL reaches – 41.7 dB with Δf = 5.5 GHz (11.1 \sim 16.6 GHz). In addition, the minimum RL (- 45.5 dB) can be obtained at a lower frequency of f = 8.14 GHz and t = 2.4 mm, in which the effective absorption bandwidth is $\Delta f = 3.49 \text{ GHz} (6.55 \sim 10.04 \text{ GHz}).$

4.4. Comparison of electromagnetic properties of magnetic materials

Magnetic properties and electromagnetic properties of typical magnetic materials used for EM wave-absorption have been summarized, and the related parameters are listed in Table S1, including $M_{\rm S}$, $H_{\rm C}$, RL_{min} , $f_{\rm m}$ matching for RL_{min} , $\varDelta f_{RL<-10dB}$, t, and the mass percentage of mixing powders/(paraffin or polyurethane) composites. The corresponding data of the current MEAs are also included in Table S1. Fig. 9 compares the EM parameters (RL_{min} , $\Delta f_{RL \le -10 dB_0}$ and t) of typical magnetic materials and the current alloys. It is found that the ferrite materials generally have good absorption performance in the low frequency band (MHz) due to the lower $M_{\rm S}$ and snoek's limit, which is evidenced by the fact the frequency band below -10 dB of the Ni-Zn ferrite is $f = 100 \sim 1000$ MHz, and the minimum RL can reach -49 dB at $f_{\rm m}$ \sim 400 MHz [38]. However, the absorption performance in the high frequency band (GHz) needs to be enhanced by combining the dielectric materials with the magnetic materials together. For instance, the reflection loss peak of NiZn-ferrite@graphene composites reaches $RL_{min} = -$ 53.5 dB at $f_{\rm m}$ = 9.6 GHz, and the effective frequency bandwidth below -10 dB is $\Delta f_{RL < -10 dB}$ = 4.8 GHz (7.2 \sim 12 GHz) at

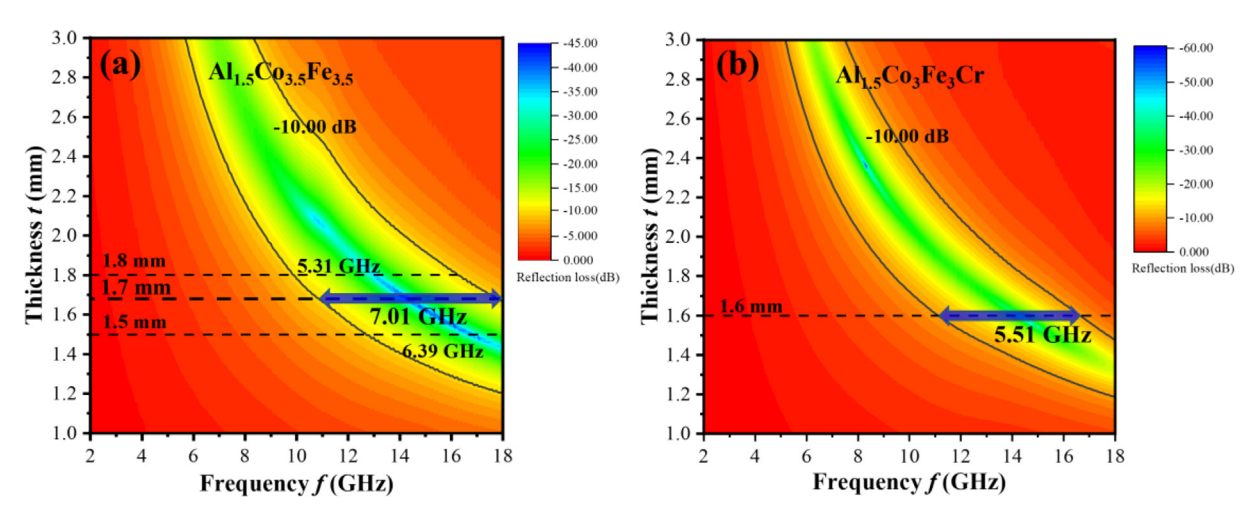


Fig. 8. Contour maps of the reflection loss RL dependent on the thickness and frequency for 5 h-milled Al_{1.5}Co_{3.5}Fe_{3.5} (a) and 10 h-milled Al_{1.5}Co₃Fe₃Cr (b) MEA powders.

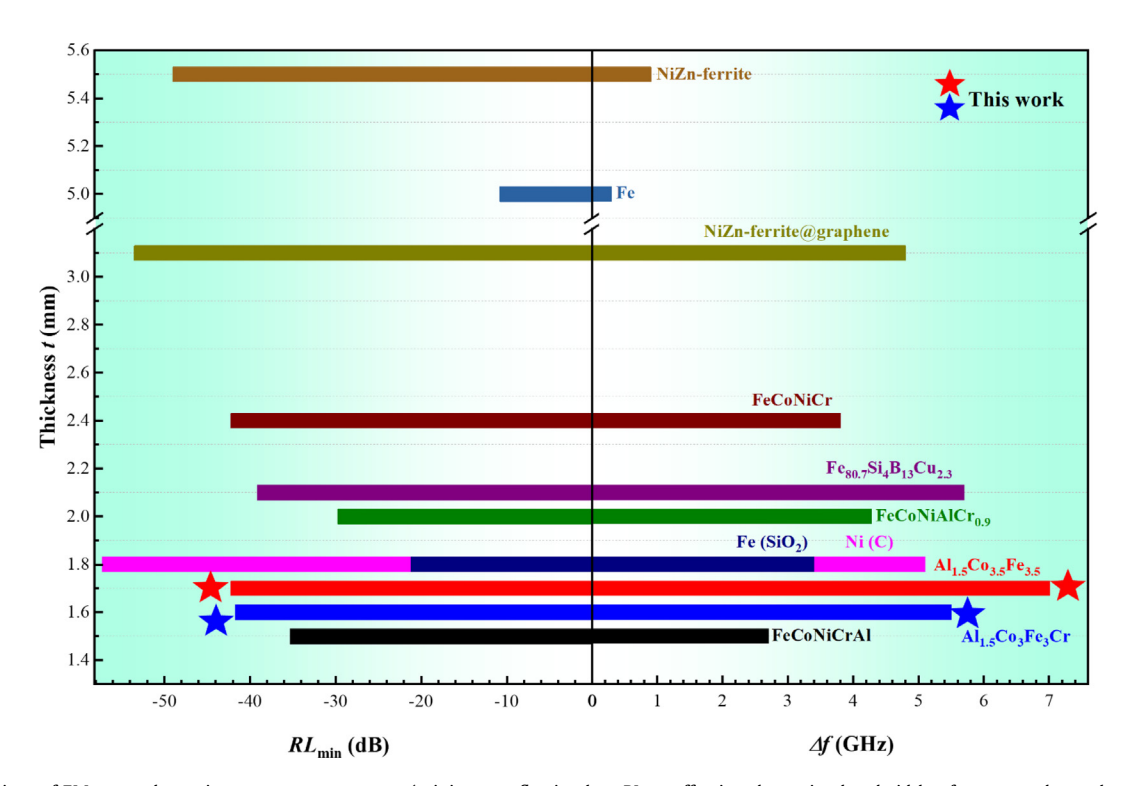


Fig. 9. Comparison of EM wave-absorption property parameters (minimum reflection loss RL_{\min} , effective absorption bandwidth $\Delta f_{RL<-10dB}$, and sample thickness t) of the typical magnetic materials and current alloy powders.

 $t=3.1~{\rm mm}$ [12]. The conventional pure metal powders have poor impedance matching due to their low resistivity and strong skin effect at high frequency, thus, the effective absorption bandwidth is generally< 2 GHz although they have high $M_{\rm S}$ (\sim 190 emu/g) [5]. Based on these, Fe (SiO₂) and Ni (C) composites with a coreshell and hollow microspheres structure could exhibit a strong electromagnetic absorption property, as exemplified by the property data of $RL_{min}=-57.25~{\rm dB}$ at $f_{\rm m}=16.1~{\rm GHz},~\Delta f_{RL<10dB}=5.1~{\rm GHz}$ (12.9 \sim 18 GHz), and $t=1.8~{\rm mm}$ for Ni(C) [2,7]. However, the mechanical property and heat resistance would be weakened in such composites [24]. By contrast, amorphousnanocrystalline soft magnetic alloys with high Fe content exhibit excellent EM wave-absorption properties, better than traditional metal powders. For instance, the Fe_{80.7}Si₄B₁₃Cu_{2.3} spherical powders with a BCC-Fe nanocrystal precipitated into the amorphous

matrix possess the minimum RL of -39.1 dB and the effective absorption bandwidth of 5.7 GHz covering the X-band (8 \sim 12 GHz) at t = 2.1 mm [17]. It is emphasized that the amorphous matrix is metastable and would be transformed to a crystalline structure when the temperature exceeds 573 K, which could deteriorate the soft-magnetic property and then EM wave-absorption property [18,19]. In addition, the existing high entropy alloy powders in Al-Fe-Co-Ni-Cr-Cu system possess relatively weak EM wave-absorption property with a narrow effective absorption bandwidth ($\Delta f_{RL<-10dB} < 5.0$ GHz), a shallow reflection loss ($RL_{min} > -40$ dB), and a too-large thickness (t > 2.0 mm), which is induced by their lower $M_{\rm S}$ and higher $H_{\rm C}$ [10,20–24]. Fascinatingly, the current $Al_{1.5}Co_{3.5}Fe_{3.5}$ and $Al_{1.5}Co_{3}Fe_{3.5}$ cr alloy powders exhibit prominent soft-magnetic property with higher $M_{\rm S}$ and lower $H_{\rm C}$, which results in a high permeability and then excellent EM wave-

absorption property with a wider $\Delta f_{RL<-10dB}$ (5.5 \sim 7.0 GHz), a deeper RL_{min} (< - 40 dB), and a thinner sample thickness (t < 2.0 mm), completely covering the Ku-band (12 \sim 18 GHz). Especially, the effective absorption bandwidth of Al_{1.5}Co_{3.5}Fe_{3.5} powers can reach up to $\Delta f_{RL<-10dB}$ = 7.01 GHz at t = 1.7 mm, exceeding significantly those of amorphous-nanocrystalline powders. Moreover, the current MEAs also have higher thermal stability at elevated temperatures (> 573 K) due to the special coherent microstructure of ultrafine BCC nanoprecipitates uniformly-distributed into the L2₁ matrix. Actually, the high thermal stability of the coherent microstructure has been demonstrated in many existing alloy systems [15,39–41].

From the above comparison, it could be concluded that the excellent electromagnetic wave-absorption property of magnetic alloy materials is dependent not only on a high permeability induced by high $M_{\rm S}$ and low $H_{\rm C}$ that corresponds to a large magnetic energy dissipation, but also on a comparable permittivity induced by high resistivity that contributes to an optimum impedance matching.

5. Conclusion

In summary, the present work investigated systematically the electromagnetic wave-absorbing property of soft-magnetic Al_{1.5}-Co_{3.5}Fe_{3.5} and Al_{1.5}Co₃Fe₃Cr medium-entropy alloy powders prepared by ball-milling. These two designed alloys exhibit a special microstructure consisting of ultrafine ferromagnetic BCC nanoparticles with a particle size of $3 \sim 8$ nm coherently precipitated in the L2₁ matrix. It is due to this kind of coherent microstructure that renders MEAs with much higher M_S (125 ~ 171 emu/g) and lower $H_{\rm C}$ (1.9 \sim 2.3 Oe). A short-time ball-milling does not change the crystalline structure of flake alloy powders, still consisting of coherent BCC and $L2_1$ phases, in which the M_S of alloy powders keeps almost constant but the H_C increases to 56 \sim 68 Oe with the balling time. In addition, these two alloys also have a high electrical resistivity, which could be further strengthened with increasing the balling time. So these two alloy powders possess excellent electromagnetic wave-absorbing properties due to the good softmagnetic property and the BCC/L2₁ coherent microstructure, better than the existing magnetic alloy materials. The deepest reflection loss and effective absorption bandwidth of 5 h-milled $Al_{1.5}Co_{3.5}Fe_{3.5}$ alloy powders are $RL_{min} = -42.2$ dB at f = 14.52 GHz and $\Delta f_{RL<-10dB}$ = 7.01 GHz (10.99 \sim 18 GHz) when the sample thickness is 1.7 mm, covering the *Ku*-band (12 \sim 18 GHz) completely.

CRediT authorship contribution statement

Zhiyao Ji: Data curation, Writing – original draft. **Qing Wang:** Conceptualization, Writing – review & editing. **Zhenhua Wang:** Investigation, Visualization. **Yuping Duan:** Methodology, Supervision. **Chuang Dong:** Conceptualization, Methodology. **Peter K. Liaw:** Supervision.

Data availability

Data will be made available on request.

Declaration of Competing Interest

The authors declare that they have no known competing financial interests or personal relationships that could have appeared to influence the work reported in this paper.

Acknowledgements

It was supported by the National Natural Science Foundation of China (52171152). PKL appreciates the supports from the National Science Foundation (DMR-1611180 and 1809640) and the US Army Research Office (W911NF-13-1-0438 and W911NF-19-2-0049).

Appendix A. Supplementary material

Supplementary data to this article can be found online at https://doi.org/10.1016/j.matdes.2022.111054.

References

- [1] A. Lqbal, F. Shahzad, K. Hantanasirisakul, M.K. Kim, J. Kwon, J. Hong, H. Kim, D. Kim, Y. Gogotsi, C.M. Koo, Anomalous absorption of electromagnetic waves by 2D transition metal carbonitride Ti₃CNT_x (MXene), Science 369 (2020) 446–450, https://doi.org/10.1126/science.aba7977.
- [2] Y. Qiu, Y. Lin, H.B. Yang, L. Wang, M.Q. Wang, B. Wen, Hollow Ni/C microspheres derived from Ni-metal organic framework for electromagnetic wave absorption, Chem. Eng. J. 383 (2020), https://doi.org/10.1016/j.cej.2019.123207 123207.
- [3] Z.C. Wu, K. Pei, L.S. Xing, X.F. Yu, W.B. You, R.C. Che, Enhanced microwave absorption performance from magnetic coupling of magnetic nanoparticles suspended within hierarchically tubular composite, Adv. Funct. Mater. 29 (2019) 1901448, https://doi.org/10.1002/adfm.201901448.
- [4] Y.P. Duan, Z. Liu, Y.H. Zhang, M. Wen, A theoretical study of the dielectric and magnetic responses of Fe-doped alpha-MnO₂ based on quantum mechanical calculations, J. Mater. Chem. C 1 (2013) 1990–1994, https://doi.org/10.1039/ c3tc00902e.
- [5] J.R. Liu, M. Itoh, T. Horikawa, E. Horikawa, E. Taguchi, H. Mori, K. Machida, Iron based carbon nanocomposites for electromagnetic wave absorber with wide bandwidth in GHz range, Appl. Phys. A-Mater. Sci. Process. 82 (2006) 509–513, https://doi.org/10.1007/s00339-005-3417-8.
- [6] T.D. Zhou, D.F. Liang, L.J. Deng, D.C. Luan, Electron structure and microwave absorbing ability of flaky FeSiAl powders, J. Mater. Sci. Technol. 27 (2011) 170– 174, https://doi.org/10.1016/S1005-0302(11)60044-3.
- [7] J.H. Zhu, S.Y. Wei, N. Haldolaarachchige, D.P. Young, Z.H. Guo, Electromagnetic field shielding polyurethane nanocomposites reinforced with core-shell Fesilica nanoparticles, J. Phys. Chem. C 115 (2011) 15304–15310, https://doi.org/ 10.1021/jp2052536.
- [8] G. Herzer, Grain size dependence of coercivity and permeability in nanocrystalline ferromagnets, IEEE Trans. Magn. 26 (1990) 1397–1402, https://doi.org/10.1109/20.104389.
- [9] J. Frenkel, J. Dorfman, Spontaneous and induced magnetisation in ferromagnetic bodies, Nature 126 (1930) 274–275, https://doi.org/10.1038/ 126274a0.
- [10] Y.P. Duan, Y.L. Cui, B. Zhang, G.J. Ma, T.M. Wang, A novel microwave absorber of FeCoNiCuAl high-entropy alloy powders: Adjusting electromagnetic performance by ball milling time and annealing, J. Alloy. Compd. 773 (2019) 194–201, https://doi.org/10.1016/j.jallcom.2018.09.096.
- [11] R.C. Pullar, Hexagonal ferrites: A review of the synthesis, properties and applications of hexaferrite ceramics, Prog. Mater. Sci. 57 (2012) 1191–1334, https://doi.org/10.1016/j.pmatsci.2012.04.001.
- [12] P.J. Liu, Z.J. Yao, J.T. Zhou, Z.H. Yang, L.B. Kong, Small magnetic Co-doped NiZn ferrite/graphene nanocomposites and their dual-region microwave absorption performance, J. Mater. Chem. C. 4 (2016) 9738–9749, https://doi.org/10.1039/ c6tc03518c.
- [13] Z. Xiang, Y.M. Song, J. Xiong, Z.B. Pan, X. Wang, L. Liu, R. Liu, H.W. Yang, W. Lu, Enhanced electromagnetic wave absorption of nanoporous Fe₃O₄@carbon composites derived from metal-organic frameworks, Carbon 142 (2019) 20– 31, https://doi.org/10.1016/j.carbon.2018.10.014.
- [14] X. Wang, F. Pan, Z. Xiao, Q.W. Zeng, K. Pei, R.C. Che, W. Lu, Magnetic vortex core-shell Fe₃O₄@C nanorings with enhanced microwave absorption performance, Carbon 157 (2020) 130–139, https://doi.org/10.1016/j.carbon.2019.10.030.
- [15] Y. Ma, Q. Wang, X.Y. Zhou, J.M. Hao, B. Gault, Q.Y. Zhang, C. Dong, T.G. Nieh, A novel soft-magnetic B2-based multiprincipal-element alloy with a uniform distribution of coherent body-centered-cubic nanoprecipitates, Adv. Mater. 33 (2021) 2006723, https://doi.org/10.1002/adma.202006723.
- [16] H.B. Kim, J.P. Jeun, S.M. Hong, P.H. Kang, Electromagnetic wave shielding effectiveness of Fe_{73.5}Si_{13.5}B₉Nb₃Cu₁ powder/epoxy composites, J. Ind. Eng. Chem. 16 (2010) 437–440, https://doi.org/10.1016/j.jiec.2009.08.010.
- [17] C.X. Zhang, Y.H. Li, Y.P. Duan, W. Zhang, Preparation and electromagnetic properties of Fe_{80.7}Si₄B₁₃Cu_{2.3} nanocrystalline alloy powders for electromagnetic wave absorbers in X-band, J. Magn. Magn. Mater. 497 (2020), https://doi.org/10.1016/j.jmmm.2019.165988 165988.
- [18] K.E. Knipling, M. Daniil, M.A. Willard, Fe-based nanocrystalline soft magnetic alloys for high-temperature applications, Appl. Phys. Lett. 95 (22) (2009) 222516

- [19] M.A. Willard, D.E. Laughlin, M.E. McHenry, D. Thoma, K. Sickafus, J.O. Cross, V. G. Harris, Structure and magnetic properties of (Fe_{0.5}Co_{0.5})₈₈Zr₇B₄Cu₁ nanocrystalline alloys, J. Appl. Phys. 84 (12) (1998) 6773–6777.
- [20] Y.P. Duan, H.F. Pang, X. Wen, X.F. Zhang, T.M. Wang, Microwave absorption performance of FeCoNiAlCr_{0.9} alloy powders by adjusting the amount of process control agent, J. Mater. Sci. Technol. 77 (2021) 209–216, https://doi. org/10.1016/j.jmst.2020.09.049.
- [21] P.P. Yang, Y. Liu, X.C. Zhao, J.W. Cheng, H. Li, Electromagnetic wave absorption properties of mechanically alloyed FeCoNiCrAl high entropy alloy powders, Adv. Powder Technol. 27 (2016) 1128–1133, https://doi.org/10.1016/j. apt.2016.03.023.
- [22] P.P. Yang, Y. Liu, X.C. Zhao, C. Zhang, Electromagnetic wave absorption properties for FeCoNiCr alloy powders with magnetic field heat treatment, J. Mater. Sci.-Mater. Electron. 28 (2017) 9867–9875, https://doi.org/10.1007/ s10854-017-6741-9.
- [23] H.J. Wu, D. Lan, B. Li, L.M. Zhang, Y. Fu, Y. Zhang, H. Xing, High-entropy alloy@air@Ni-NiO core-shell microspheres for electromagnetic absorption applications, Compos. Pt. B-Eng. 179 (2019), https://doi.org/10.1016/ j.compositesb.2019.107524 107524.
- [24] D. Lan, Z.H. Zhao, Z.G. Gao, K.C. Kou, G.L. Wu, H.J. Wu, Porous high entropy alloys for electromagnetic wave absorption, J. Magn. Magn. Mater. 512 (2020), https://doi.org/10.1016/j.jmmm.2020.167065 167065.
- [25] C.M. Liu, H.M. Wang, S.Q. Zhang, H.B. Tang, A.L. Zhang, Microstructure and oxidation behavior of new refractory high entropy alloys, J. Alloy. Compd. 583 (2014) 162–169, https://doi.org/10.1016/j.jallcom.2013.08.102.
- [26] Y.Z. Shi, L. Collins, R. Feng, C. Zhang, N. Balke, P.K. Liaw, B. Yang, Homogenization of AlxCoCrFeNi high-entropy alloys with improved corrosion resistance, Corrosion Sci. 133 (2018) 120–131, https://doi.org/ 10.1016/j.corsci.2018.01.030.
- [27] C.A. Schneider, W.S. Rasband, K.W. Eliceiri, 50 Years of Image Analysis, Nat. Methods 9 (2012) 671–675.
- [28] A.M. Li, D. Ma, Q.F. Zheng, Effect of Cr on Microstructure and Properties of a Series of AlTiCr_xFeCoNiCu High-Entropy Alloys, J. Mater. Eng. Perform. 23 (2014) 1197–1203, https://doi.org/10.1007/s11665-014-0871-5.
- [29] J.W. Yeh, S.K. Chen, S.J. Lin, J.Y. Gan, T.S. Chin, T.T. Shun, C.H. Tsau, S.Y. Chang, Nanostructured high-entropy alloys with multiple principal elements: novel alloy design concepts and outcomes, Adv. Eng. Mater. 6 (2004) 299–303, https://doi.org/10.1002/adem.200300567.
- [30] B. Gludovatz, A. Hohenwarter, D. Catoor, E.H. Chang, E.P. George, R.O. Ritchie, A fracture-resistant high-entropy alloy for cryogenic applications, Science 345 (2014) 1153–1158, https://doi.org/10.1126/science.1254581.

- [31] D.B. Miracle, O.N. Senkov, A critical review of high entropy alloys and related concepts, Acta Mater. 122 (2016) 448–511, https://doi.org/10.1016/j. actamat 2016 08 081
- [32] S. Huang, W. Li, X.Q. Li, S. Schonecker, L. Bergqvist, E. Holmstrom, L.K. Varga, L. Vitos, Mechanism of magnetic transition in FeCrCoNi-based high entropy alloys, Mater. Des. 103 (2016) 71–74, https://doi.org/10.1016/j.matdes.2016.04.053.
- [33] Y. Yoshizawa, S. Oguma, K. Yamauchi, New Fe-based soft magnetic alloys composed of ultrafine grain structure, J. Appl. Phys. 64 (1988) 6044–6046, https://doi.org/10.1063/1.342149.
- [34] G. Herzer, Modern soft magnets: Amorphous and nanocrystalline materials, Acta Mater. 61 (2013) 718–734, https://doi.org/10.1016/j.actamat.2012.10.040.
- [35] Y. Wu, M. Han, Z. Tang, L. Deng, Eddy current effect on the microwave permeability of Fe-based nanocrystalline flakes with different sizes, J. Appl. Phys. 115 (16) (2014) 163902.
- [36] X. Luo, Y.H. Wu, M.G. Han, L.J. Deng, High frequency permeability of Fe-Cu-Nb-Si-B nanocrystalline flakes with the distribution of shape anisotropy fields, J. Magn. Magn. Mater. 451 (2018) 5–10, https://doi.org/10.1016/j.jmmm.2017.10.113.
- [37] S.S. Kim, S.B. Jo, K.I. Gueon, K.K. Choi, J.M. Kim, K.S. Churn, Complex permeability and permittivity and microwave absorption of ferrite-rubber composite in X-band frequencies, IEEE Trans. Magn. 27 (1991) 5462–5464, https://doi.org/10.1109/20.278872.
- [38] Y. Hwang, Microwave absorbing properties of NiZn-ferrite synthesized from waste iron oxide catalyst, Mater. Lett. 60 (2006) 3277–3280, https://doi.org/ 10.1016/j.matlet.2006.03.010.
- [39] Z.M. Li, X.N. Li, Y.L. Hu, Y.H. Zheng, M. Yang, N.J. Li, L.X. Bi, R.W. Liu, Q. Wang, C. Dong, Y.X. Jiang, X.W. Zhang, Cuboidal γ' phase coherent precipitation-strengthened Cu-Ni-Al alloys with high softening temperature, Acta Mater. 203 (2021), https://doi.org/10.1016/j.actamat.2020.10.076 116458.
- [40] Z.H. Wang, B. Niu, Q. Wang, C. Dong, J.C. Jie, T.M. Wang, T.G. Nieh, Designing ultrastrong maraging stainless steels with improved uniform plastic strain via controlled precipitation of coherent nanoparticles, J. Mater. Sci. Technol. 93 (2021) 60–70, https://doi.org/10.1016/j.jmst.2021.04.011.
- [41] Y. Ma, Q. Wang, B.B. Jiang, C.L. Li, J.M. Hao, X.N. Li, C. Dong, T.G. Nieh, Controlled formation of coherent cuboidal nanoprecipitates in body-centered cubic high-entropy alloys based on Al₂(Ni Co, Fe, C_r)₁₄ compositions, Acta Mater. 147 (2018) 213–225, https://doi.org/10.1016/j.actamat.2018.01.050.